

Optical Engineering

SPIDigitalLibrary.org/oe

Real-time single-shot measurement and correction of pulse phase and amplitude for ultrafast lasers

Dmitry Pestov
Anton Ryabtsev
Gennady Rasskazov
Vadim V. Lozovoy
Marcos Dantus

Real-time single-shot measurement and correction of pulse phase and amplitude for ultrafast lasers

Dmitry Pestov,^a Anton Ryabtsev,^b Gennady Rasskazov,^b Vadim V. Lozovoy,^b and Marcos Dantus^{b,*}

^aBiophotonic Solution, Inc, 1401 East Lansing Drive, Suite 112, East Lansing, Michigan 48823

^bMichigan State University, Department of Chemistry, East Lansing, Michigan 48824

Abstract. The transition of femtosecond lasers from the laboratory to commercial applications requires real-time automated pulse compression, ensuring optimum performance without assistance. Single-shot phase measurements together with closed-loop optimization based on real-time multiphoton intrapulse interference phase scan are demonstrated. On-the-fly correction of amplitude, as well as second- and third-order phase distortions based on the real-time measurements, is accomplished by a pulse shaper. © 2014 Society of Photo-Optical Instrumentation Engineers (SPIE) [DOI: 10.1117/1.OE.53.5.051511]

Keywords: femtosecond phenomena; lasers; phase measurement; pulse shaping.

Paper 131295SS received Aug. 21, 2013; revised manuscript received Dec. 4, 2013; accepted for publication Dec. 6, 2013; published online Jan. 9, 2014.

1 Introduction

Femtosecond laser systems are being used for an increasingly large number of applications given their ability to deliver high-peak power densities (from 10^{10} to 10^{16} W/cm²) with very modest pulse energies (from 10^{-12} to 10^{-3} J). Some of these technologies have transferred from the research laboratory to commercial applications, for example, femtosecond refractive surgery,¹ cataracts surgery,² and material processing.^{3,4} Although the laser sources have experienced great progress in terms of output pulse characteristics, reliability, and size, they are still notoriously complex and sensitive to changes in ambient environment. In addition to the static dispersion introduced by the laser components themselves and high-numerical-aperture microscope objectives, modern ultrafast laser design needs to take into account laser-induced nonlinear optical processes, such as self-phase modulation⁵ and laser-induced group velocity dispersion.⁶ As a result, minute changes in power, cavity length, or alignment lead to deterioration in pulse characteristics. Applications of femtosecond lasers outside of laser laboratories thus require automated dispersion and amplitude drift characterization and compensation in order to maintain optimum performance without human assistance. If this can be accomplished, femtosecond lasers, ranging from commercial high-repetition rate units to high-intensity petawatt class lasers,⁷ could certainly benefit from the technology.

It is possible to achieve some degree of automated pulse optimization without using pulse characterization. Given that the integrated second-harmonic-generation (SHG) intensity achieves a maximum value for transform limited (TL) pulses, this intensity can be used as feedback for a closed loop, while the pulse shaper introduces hundreds of different phases with the goal of converging towards the shortest pulses.^{8,9} Unfortunately, the process is time consuming and the degree of success of this approach depends on the square of the noise level of the laser system. For many cases, it is sufficient to optimize chirp by feeding back the integrated SHG intensity to a prism or grating compressor,¹⁰ an approach that has

been adopted by some commercial systems. Given that tracking SHG intensity does not provide sufficient phase information, these systems require dithering the chirp to find the optimum value. Ideally, phase optimization is based on accurate phase characterization.

Measuring phase distortions requires pulse characterization, on-the-fly correction requires single-shot pulse characterization; a topic that has received considerable attention since the early 1990s.^{11–15} Following the single-shot pulse characterization, the information needs to be processed and used to actuate optics in the laser compressor or to a pulse shaper. Operationally, phase drifts manifest themselves in nonlinear phase distortion, primarily in the second- and sometimes third-order distortion of the spectral phase (SOD and TOD, respectively). Therefore, a method is needed to directly provide quantitative SOD and TOD information with minimal use of time-consuming phase retrieval algorithms.

Here, we take advantage of the inherent sensitivity of nonlinear optical processes to phase distortions. This sensitivity, in particular to SOD and TOD, was discussed in the context of multiphoton intrapulse interference for control of two- and three-photon laser induced processes.¹⁶ In that article, it was noted that the TOD leads to narrowing of the SHG spectrum and the addition of SOD leads to a shift of the maximum SHG to longer wavelengths (when both are positive). This sensitivity was used to develop multiphoton intrapulse interference phase scan (MIIPS),^{17,18} a method that combines the introduction of one or more known spectral phases to measure the unknown phase of a laser pulse, and once the measurement is complete, introduce the measured phase distortion with opposite sign to obtain TL pulses. The application of coherent quantum control to shift the frequency where maximum nonlinear optical processes take place,¹⁶ for example in multiphoton excitation, has been patented and used for a number of applications such as selective two-photon microscopy.^{19,20} Here, we extract SOD and TOD values from changes in the SHG spectrum. It is worth noting

*Address all correspondence to: Marcos Dantus, E-mail: dantus@msu.edu

that here we are not proposing a pulse characterization method for arbitrary phase distortions in a previously uncharacterized laser pulse. The intention of our work is to measure and correct small deviations in SOD and TOD occurring in laser system over time. The real-time version of multiphoton intrapulse interference phase scan (RT-MIIPS) proposed is for monitoring and stabilization of pulse energies and peak powers for optimum unattended ultrafast laser performance over an indefinite period of time. Results from this work were first presented at the 2011 Ultrafast Optics UFO VIII Conference.

2 Principle of RT-MIIPS Measurement of SOD

The principle behind our method hinges on the fact that TOD causes a narrowing of the SHG spectrum but the maximum value remains at $2\omega_0$; however, addition of SOD causes a shift in the position of the maximum SHG due to multiphoton intrapulse interference (MII) at shorter or longer SHG wavelengths (depending on the SOD sign), as illustrated in Fig. 1.¹⁶ In this work, we use a home-built Yb-doped fiber oscillator.²¹

A plot of group delay, such as the one shown in Fig. 1, shows the time-domain relationship between spectral components of the laser pulse. We observe that SHG spectrum is narrowed compared to that of a TL pulse when the spectral phase has a significant amount of TOD (cubic) because the group delay, which is the first derivative of spectral phase with respect to frequency, has a parabolic shape [Fig. 1(a), color curves]. All spectral components symmetrically around the peak of the parabola are equally delayed, with delay increasing toward the wings of the parabola. Components with equal delay produce an efficient constructive MII; however, as the relative delay increases, destructive interference takes place resulting in a narrow peak in the SHG spectrum. If TOD and consequently group delay is centered around laser central wavelength [Fig. 1(a), triangles], the resulting peak will appear in the middle of a spectral range, corresponding to the peak position of the SHG spectrum at TL pulse [Fig. 1(b), triangles and gray solid lines, respectively]. Adding of SOD to a spectral phase is equal to adding a linear group delay term which shifts parabola to shorter or longer wavelengths for negative and positive SOD, respectively [Fig. 1(a), circles and diamonds]. Shift of the group-delay

parabola results in corresponding spectral SHG shifts [Fig. 1(b), circles and diamonds].

The described behavior can be inferred from a mathematical analysis where the local maximum in the SHG spectrum at frequency $\omega_{\max}^{\text{SHG}} = 2\omega_{\max}$, where ω_{\max} is a fundamental frequency, corresponds to the spectral phase $\phi(\omega)$ of the fundamental spectrum that satisfies the relation:

$$\left. \frac{d^2\phi(\omega)}{d\omega^2} \right|_{\omega=\omega_{\max}} = 0. \quad (1)$$

The spectral phase with TOD only can be written as

$$\phi(\omega) = \frac{\phi_3 \cdot (\omega - \omega_0)^3}{6}, \quad (2)$$

where ω_0 is the central frequency of the fundamental laser spectrum and $\phi_3 = d^3\phi(\omega)/d\omega^3$ is the TOD. Substitution of Eq. (2) into Eq. (1) results in $\phi_3 \cdot (\omega_{\max} - \omega_0) = 0$, which gives a local maximum in the SHG spectrum at $\omega_{\max}^{\text{SHG}} = 2\omega_0$. When some amount of SOD ($\phi_2 = d^2\phi(\omega)/d\omega^2$) is added, the spectral phase can be written as

$$\phi(\omega) = \frac{\phi_3 \cdot (\omega - \omega_0)^3}{6} + \frac{\phi_2 \cdot (\omega - \omega_0)^2}{2}. \quad (3)$$

Substitution of Eq. (3) into Eq. (1) results in $\phi_2 + \phi_3 \cdot (\omega_{\max} - \omega_0) = 0$, i.e., the SHG peak shifts to $\omega_{\max}^{\text{SHG}} = 2 \cdot (\omega_0 - \phi_2/\phi_3)$. Therefore, SOD changes are correlated with SHG peak shifts according to

$$\Delta\omega_{\max}^{\text{SHG}} = -2 \cdot \phi_2/\phi_3. \quad (4)$$

From Eq. (4), it follows that for a given positive TOD, the observed SHG spectrum peak shifts to shorter wavelengths when negative SOD is acquired by the pulse and vice versa. Given that laser pulses have spectra that are not ideal Gaussian functions, the method should be calibrated on the actual laser system to provide the most accurate results. The work was carried out using a home-built Yb-doped fiber oscillator producing sub-45 fs²¹ and a reflective 4f pulse

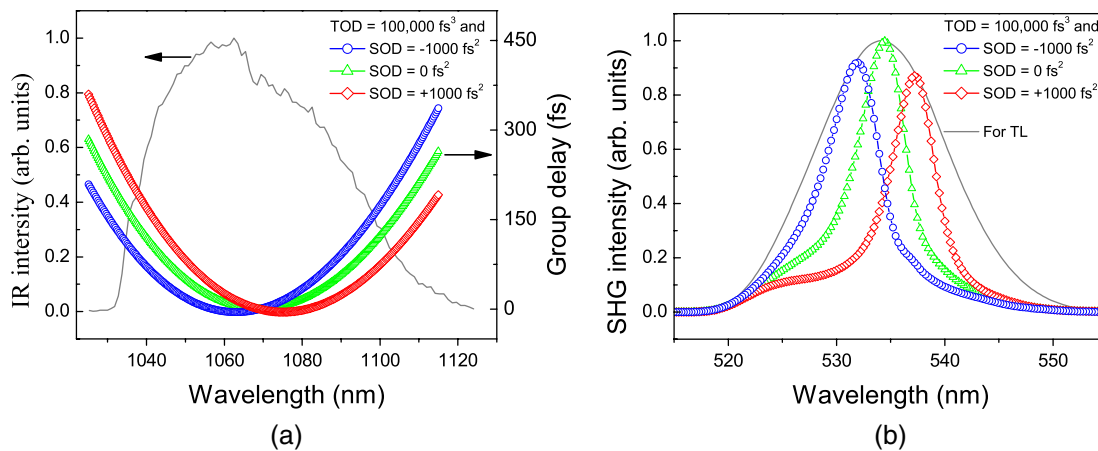


Fig. 1 Principle of the real-time multiphoton intrapulse interference phase scan (RT-MIIPS) measurement of SOD. (a) The experimental IR spectrum (black curve) from the Yb-doped fiber laser and the group delay curves corresponding to three spectral phases with different SOD values (see legend) and a fixed amount of TOD. (b) The SHG spectra calculated using the spectrum and phases from (a).

shaper (MIIPSBox640, Biophotonic Solutions Inc., East Lansing, Michigan). It is best to start with fully characterized pulses, which can be achieved by simply scanning SOD.^{22,23} The SHG spectrum for transform-limited pulses of the Yb fiber laser here covers the 515- to 555-nm range (bottom-to-bottom). The first step is to impose a reference phase mask with some amount of TOD to narrow SHG spectrum, which can be done with the pulse shaper or by introducing a dispersive optical element with the desired characteristics.⁶ Here, the cubic reference phase of $+100,000 \text{ fs}^3$ is applied using a reflective $4f$ pulse shaper. The second step is to acquire a two-dimensional spectrogram as a function of linear chirped (Fig. 2). The third step is to extract the position of the maximum SHG for each SOD value. Here, we implement weighted averaging over spectral points above a fixed threshold to reduce the noise and achieve sub-spectrometer-limited resolution.

The wavelength of maximum SHG intensity as a function of SOD is fitted by a second-order polynomial, yielding the calibration curve. Once the one-to-one correspondence is established, one can accurately measure changes in SOD by acquiring a single SHG spectrum, and if the measurement corresponds to an undesired drift, the system can correct it. The standard deviation for the measured SOD values is found to be about 60 fs^2 . It is worth noting that RT-MIIPS relies on spectroscopic changes in SHG (peak shifts) rather than on the intensity of SHG. Fluctuations in SHG intensity caused by noise limit integrated SHG-based methods. For instance, potentially minimal 2% fluctuations in integrated SHG result in uncertainty of $\pm 150 \text{ fs}^2$ of SOD in a 40-fs pulse. A long-term loss of intensity, for instance, due to pump diode power drifts/degradation, changes in reflection/transmission of optical elements, would cause a systematic phase error. RT-MIIPS, in contrast to SHG intensity based methods, is not sensitive to intensity fluctuations. Its sensitivity is limited by the spectrometer resolution; therefore, it can be used with very low laser intensities.

3 Principle of RT-MIIPS Measurement of TOD

To measure and correct for both SOD and TOD, we have modified the reference phase to incorporate two cubic

phase masks, which are offset spectrally, therefore, they have different group-delay terms. The corresponding group delay for this reference phase consists of two parabolas [shown schematically in Fig. 3(a)]. Mathematically, the reference phase function can be written as

$$\varphi_{\text{ref}}(\omega) = \begin{cases} \frac{\varphi_3}{6}(\omega - \omega_1)^3 + \tau \cdot (\omega - \omega_1) & \text{if } \omega < \omega_0, \\ -\frac{\varphi_3}{6}(\omega - \omega_2)^3 - \tau \cdot (\omega - \omega_2) & \text{if } \omega \geq \omega_0. \end{cases} \quad (5)$$

Here, ω_1 and ω_2 are two frequencies within the spectrum equally offset from ω_0 ($\omega_1 < \omega_0$ and $\omega_2 > \omega_0$). Note that these are “zero dispersion” frequencies if no phase distortion is present. In practice, they are defined through the corresponding wavelengths λ_1 and λ_2 , which are calculated from the center wavelength λ_0 and offset $\Delta\lambda$ in nanometers

$$\lambda_{1,2} = \frac{1}{2} \times \left(\lambda_0 \pm \Delta\lambda + \sqrt{\lambda_0^2 + \Delta\lambda^2} \right). \quad (6)$$

The amount of TOD (φ_3) introduced defines the sharpness of the local maxima in the SHG spectrum due to MI. The nonzero time delay τ allows suppressing sum of the frequency generation. The SHG spectrum due to the reference phase exhibits two local maxima, each corresponding to a different group delay parabola, as shown in Fig. 3(b). Due to the offset of the zero-dispersion points from the center (here, $\lambda_0 = 1070 \text{ nm}$, $\Delta\lambda = 30 \text{ nm}$), the maxima positions are affected by both SOD and TOD phase distortions and one can isolate the two contributions.

Indeed, if we define ω_A and ω_B as zero dispersion frequencies in the presence of nonzero phase distortion, the corresponding TOD ($\delta\varphi_3$) and SOD ($\delta\varphi_2$) drifts can be expressed as

$$\begin{cases} \delta\varphi_3 = \varphi_3 \cdot \frac{\Delta\omega_B + \Delta\omega_A}{\omega_B - \omega_A}, \\ \delta\varphi_2 = \frac{\varphi_3}{2} \cdot \frac{\Delta\omega_B - \Delta\omega_A}{\omega_B - \omega_A} - \frac{\varphi_3}{2} \cdot \frac{(\Delta\omega_B + \Delta\omega_A)^2}{\omega_B - \omega_A}, \end{cases}$$

where $\Delta\omega_A = \omega_A - \omega_1$ and $\Delta\omega_B = \omega_B - \omega_2$. If they are equal to zero, there is no phase distortion. Qualitatively, pure SOD distortions ($\delta\varphi_3 = 0$) shift the two SHG peaks

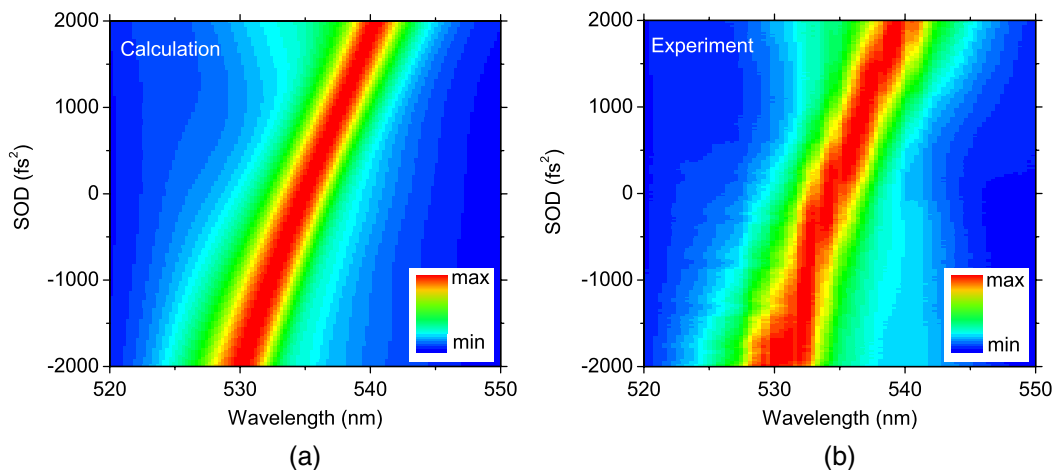


Fig. 2 RT-MIIPS calibration for SOD measurements. (a) The SHG spectrogram calculated using the experimental laser spectrum. (b) Experimental SHG spectrogram. Calculated and experimental spectra correspond to a set of polynomial phases with SOD ranging from $-2,000$ to $2,000 \text{ fs}^2$ (scanned) and TOD of $100,000 \text{ fs}^3$ (fixed). Every SHG spectrum is normalized.

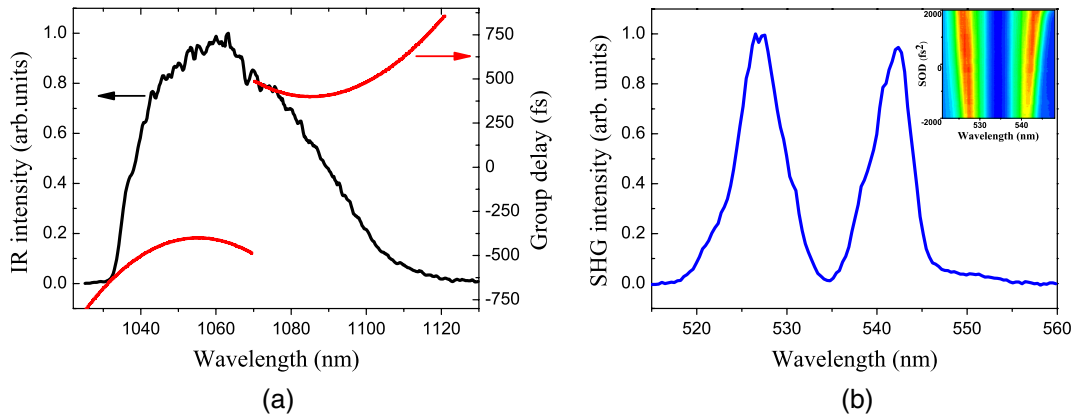


Fig. 3 Principle of RT-MIIPS measurement of SOD and TOD. (a) Fiber laser fundamental spectrum and group delay corresponding to the reference phase mask (two incorporated cubic phase masks, see text). (b) SHG spectrum corresponding to the reference phase mask from (a). Inset: SHG spectrogram with SOD scanned from -2000 fs^2 to 2000 fs^2 .

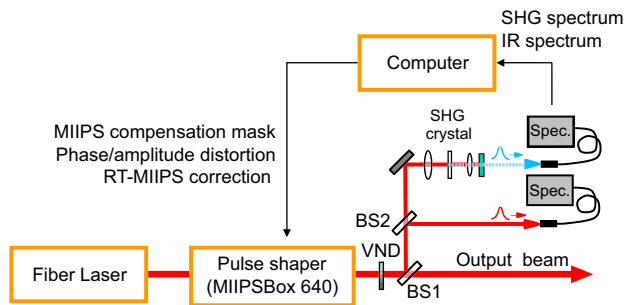


Fig. 4 RT-MIIPS setup. VND, variable neutral density filter; BS1,2, beam splitters.

in the opposite directions and by the same amount $\Delta\omega_B = -\Delta\omega_A$. Pure TOD distortions move the peaks in the same direction.

As in the SOD measurements, RT-MIIPS TOD measurement is calibrated by running a linear chirp scan and recording the SHG spectra. The weighted SHG spectral peak positions, as a function of chirp, are then fitted with polynomials. The calibration data shown in Fig. 3(b, inset), corresponds to a linear chirp scan from -2000 to 2000 fs^2 . The reference phase parameters are $\lambda_0 = 1070$ nm; $\Delta\lambda = 30$ nm; $\varphi_3 = 300,000$ fs^3 ; and delay $\tau = 400$ fs. The weighted SHG peak positions are fitted with third-order polynomials. The standard deviations for the measured SOD and TOD values

are found to be about 100 fs^2 and 4000 fs^3 , respectively. Again, the method proves to be more sensitive than measurements of integrated intensity.

4 Experiment

The experimental setup is shown schematically in Fig. 4. The reflective pulse shaper is used to control phase and amplitude, and also to correct changes in phase and amplitude based on the closed-loop feedback. A small portion of laser beam from the laser output is split for monitoring the fundamental IR spectrum, and after frequency doubling in nonlinear crystal, for SHG spectrum acquisition (both by Ocean Optics USB4000 spectrometers). Although this setup can be greatly simplified, we need the maximum flexibility for our first laboratory test.

To validate the performance of active phase monitoring and correction, we carried out several test experiments. In one of them, we inserted in and out of the beam path a 30-mm thick piece of fused silica (Fig. 5). Calculations based on the Sellmeier's equation give for fused silica 16 fs^2/mm of SOD at 1070 nm, i.e., about 480 fs^2 for the optic. The compensation routine measures it to be 450 ± 80 fs^2 [Fig. 5(a)]. As an indicator of pulse quality, we use SHG signal intensity. All spectra were taken within a single data acquisition cycle. Each cycle took about 100 ms to complete, limited by the spatial light modulator response time. As expected, SHG signal drops when the fused silica sample

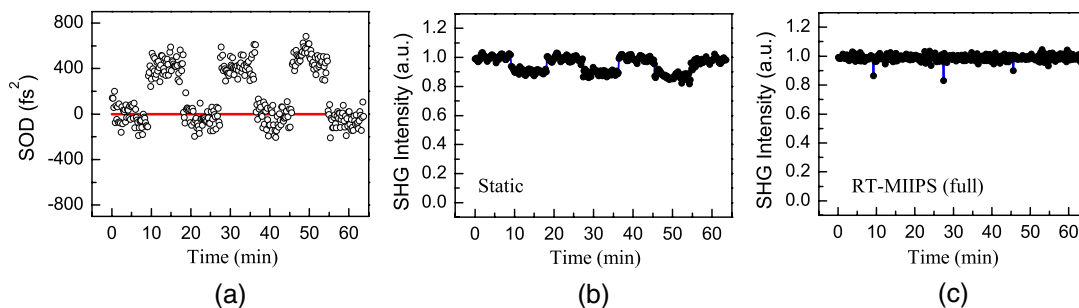


Fig. 5 Validation of RT-MIIPS response to the insertion of a dispersive optical element. (a) SOD measured by RT-MIIPS. (b) Integrated SHG intensity (RT-MIIPS compensation off). (c) Integrated SHG intensity with RT-MIIPS compensation. All data are taken in the same acquisition cycle.

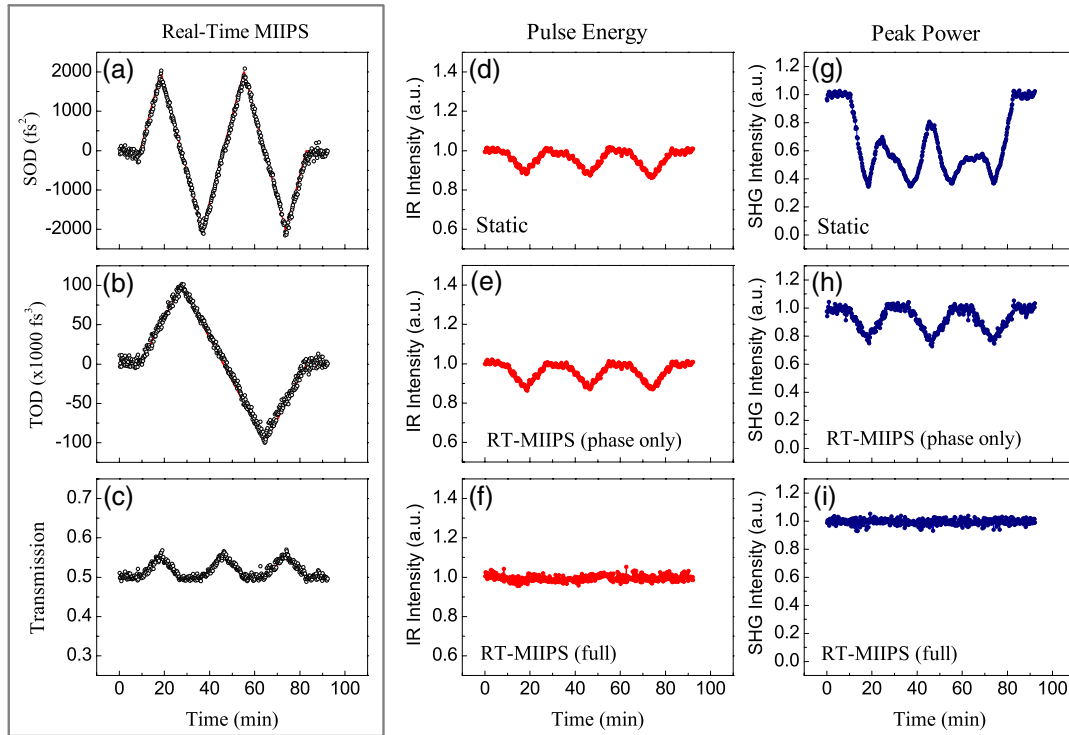


Fig. 6 Validation of RT-MIIPS response to continuous sweeping of SOD, TOD, and amplitude: (a) Measured SOD, swept by the shaper; (b) measured TOD, swept by the shaper; (c) applied transmission mask, swept by the shaper by as much as 10%; (d)–(f) integrated IR spectra for (d) static phase compensation and transmission masks; (e) RT-MIIPS corrected phase and static transmission masks; and (f) RT-MIIPS corrected phase and transmission masks. (g)–(i) Integrated SHG spectra for (g) static phase compensation and transmission masks; (h) RT-MIIPS corrected phase and static transmission masks; and (i) RT-MIIPS corrected phase and transmission masks.

is inserted due to group delay distortion [Fig. 5(b)]. When we activate the feedback loop, the pulse shaper applies a phase mask with a negative value to the measured SOD, thus recovering the original SHG intensity as shown in Fig. 5(c).

The next comprehensive test applies well-characterized phase distortions, simultaneous sweeping of SOD and

TOD and amplitude attenuation performed by the pulse shaper. The functions for SOD, TOD, and amplitude introduced are shown in the first column in Fig. 6. The second column in Fig. 6 shows the pulse energy, which varies as a function of the changes in amplitude introduced [Fig. 6(c)]. The peak power, monitored as integrated SHG intensity

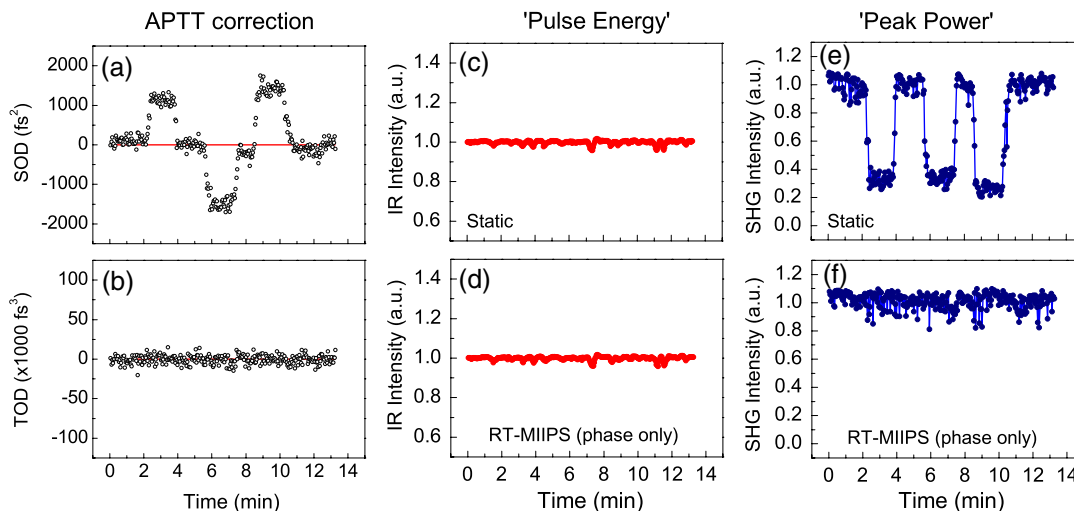


Fig. 7 Validation of RT-MIIPS response to abrupt phase distortions introduced by the amplifier compressor: (a) measured SOD change; (b) measured TOD change; (c) and (d) integrated IR spectra for static phase compensation and RT-MIIPS corrected phase, respectively; (e) and (f) integrated SHG spectra for static phase compensation and RT-MIIPS corrected phase.

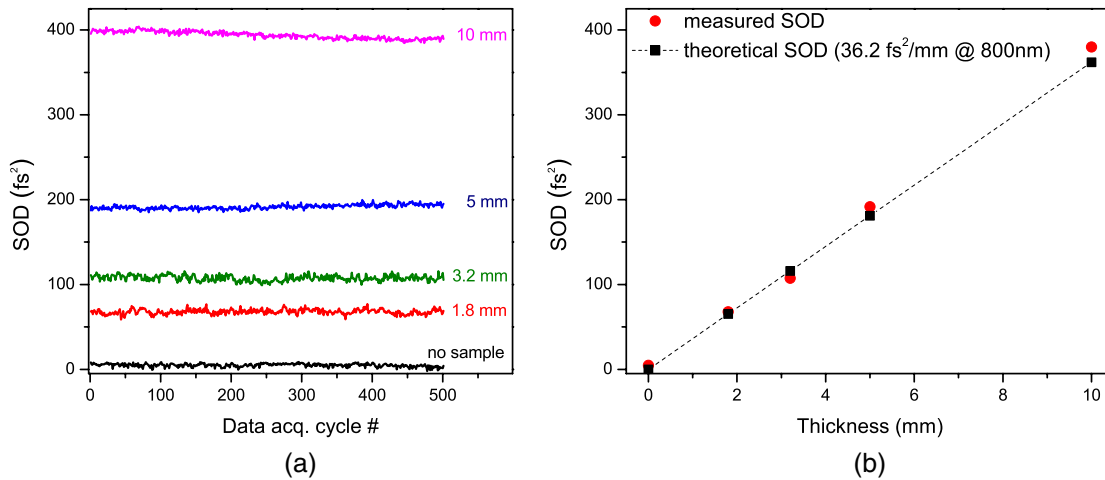


Fig. 8 Chromatic dispersion measurements of fused silica: (a) measured SOD as a function of time for four different samples: 1.8, 3.2, 5, and 10 mm and (b) measured SOD as a function of thickness. Squares represent calculated values of SOD for corresponding samples.

varies according to phase and amplitude, as shown in Fig. 6(g). When the feedback loop is allowed to compensate for phase, there is a significant improvement in the integrated SHG intensity [Fig. 6(h)]. When phase and amplitude are corrected, the SHG intensity remains stable despite the SOD, TOD, and amplitude variations introduced. Note that given the measurement of sign and amplitude of SOD and TOD, there is no need for dithering and there is no evidence of overshooting in the closed-loop correction. The accuracy and stability of RT-MIIPS can be realized from close inspection of the first column in Figs. 6(a)–6(c), where the introduced phase and amplitude variations are shown as solid line and the experimental correction (with reverse sign) as shown as gray circles.

In order to provide additional validation of the phase measurement and correction capabilities of RT-MIIPS, we present results for different laser systems. In the next experiment, we have introduced phase distortion by adjusting the Ti:Sapphire regenerative amplifier compressor (Spitfire, Spectra-Physics, Santa Clara, California), namely changing the distance between its gratings by means of built-in controllable linear stage. The detection setup is similar to Fig. 4, and the pulse shaper is placed between oscillator and amplifier. Dispersion jumps were introduced for this case by changing the grating spacing in the compressor. The results from this run are presented in Fig. 7. For these experiments, RT-MIIPS measures changes in the phase [Fig. 7(a)], which result in significant (70%) drop in peak power [Fig. 7(e)]; however, the pulse shaper automatically compensates the phase distortions and is able to maintain the peak power constant [Fig. 7(f)]. The fluctuations in peak power after compensation are inherent to the laser and are not caused by RT-MIIPS.

In general, RT-MIIPS measures any fluctuations of in the spectral phase including those intrinsic to the laser system. For the following experiments, we used a regenerative amplifier system similar to the one used for the previous experiments but with a more stable output (Micra Seed with Legend Amplifier, Coherent Inc., Santa Clara, California). We inserted four fused silica samples with different thicknesses in the laser path after the amplifier. The dispersion

introduced by each sample was measured in 500 acquisition cycles. Each cycle took about 100 ms, and the results are presented in Fig. 8. The measurements turn out to be very precise with standard deviation within 4.2 fs^2 . The accuracy is in a good agreement with theoretical values as shown in Fig. 8.

5 Conclusion

To summarize, we demonstrate a method for real-time measurement and correction of amplitude as well as second- and third-order spectral phase distortions of ultrashort optical pulses. The single-shot phase measurement exploits the well-understood dependence of the SHG spectrum on spectral phase. The current implementation is based on a programmable pulse shaper. It is worth noting that both measurement and compression can be achieved without a pulse shaper. The implementation of MIIPS by translating and tilting the grating in a compressor, shown by Hou et al.,²³ could easily be part of the closed-loop approach demonstrated here. The encoding of the cubic reference phase can be achieved by using dielectric optics with desired characteristics or simply taking advantage of the cubic phase inherent to some optics like microscope objectives. The method shown here would be ideal for correction of phase and amplitude drifts in commercial laser systems (oscillators and amplifiers), to provide greater unassisted long-term performance. An application of RT-MIIPS being pursued in our laboratory, which takes advantage of its ability to measure laser-induced phase distortions, is quantifying laser-induced group delay dispersion,⁶ and time-domain pulse shaping.²⁴

Acknowledgments

This work was funded in part by Navy SBIR Program (Contract # N68335-11C-0153) and CHE-1014538 Early-Concept Grant for Exploratory Research from the NSF.

References

1. T. Juhasz et al., "Corneal refractive surgery with femtosecond lasers," *IEEE J. Sel. Top. Quant.* 5(4), 902–910 (1999).

2. R. R. Krueger et al., "First safety study of femtosecond laser photo-disruption in animal lenses: Tissue morphology and cataractogenesis," *J. Cataract Refr. Surg.* **31**(12), 2386–2394 (2005).
3. B. N. Chichkov et al., "Femtosecond, picosecond and nanosecond laser ablation of solids," *Appl. Phys. A Mater.* **63**(2), 109–115 (1996).
4. X. Liu, D. Du, and G. Mourou, "Laser ablation and micromachining with ultrashort laser pulses," *IEEE J. Quant. Electron.* **33**(10), 1706–1716 (1997).
5. F. Krausz et al., "Femtosecond solid-state lasers," *IEEE J. Quant. Electron.* **28**(10), 2097–2122 (1992).
6. G. Rasskazov et al., "Anomalous laser-induced group velocity dispersion in fused silica," *Opt. Express* **21**(15), 17695–17700 (2013).
7. T. Ditmire et al., "Overview of future directions in high energy-density and high-field science using ultra-intense lasers," *Radiat. Phys. Chem.* **70**(4–5), 535–552 (2004).
8. D. Yelin, D. Meshulach, and Y. Silberberg, "Adaptive femtosecond pulse compression," *Opt. Lett.* **22**(23), 1793–1795 (1997).
9. T. Baumert et al., "Femtosecond pulse shaping by an evolutionary algorithm with feedback," *Appl. Phys. B Lasers Opt.* **65**(6), 779–782 (1997).
10. M. M. Mielke et al., "Pulse width stabilization for ultrafast laser systems," *Phys. Procedia* **12**(Part B), 437–444 (2011).
11. A. Brun et al., "Single-shot characterization of ultrashort light-pulses," *J. Phys. D Appl. Phys.* **24**(8), 1225–1233 (1991).
12. D. J. Kane, "Recent progress toward real-time measurement of ultrashort laser pulses," *IEEE J. Quant. Electron.* **35**(4), 421–431 (1999).
13. T. M. Shuman et al., "Real-time SPIDER: ultrashort pulse characterization at 20 Hz," *Opt. Express* **5**(6), 134–143 (1999).
14. V. R. Supradeepa, D. E. Leaird, and A. M. Weiner, "Single shot amplitude and phase characterization of optical arbitrary waveforms," *Opt. Express* **17**(16), 14434–14443 (2009).
15. M. Lelek et al., "Time resolved spectral interferometry for single shot femtosecond characterization," *Opt. Commun.* **261**(1), 124–129 (2006).
16. V. V. Lozovoy et al., "Multiphoton intrapulse interference. II. Control of two- and three-photon laser induced fluorescence with shaped pulses," *J. Chem. Phys.* **118**(7), 3187–3196 (2003).
17. Y. Coello et al., "Interference without an interferometer: a different approach to measuring, compressing, and shaping ultrashort laser pulses," *J. Opt. Soc. Am. B* **25**(6), A140–A150 (2008).
18. V. V. Lozovoy, I. Pastirk, and M. Dantus, "Multiphoton intrapulse interference. IV. Ultrashort laser pulse spectral phase characterization and compensation," *Opt. Lett.* **29**(7), 775–777 (2004).
19. I. Pastirk et al., "Selective two-photon microscopy with shaped femtosecond pulses," *Opt. Express* **11**(14), 1695–1701 (2003).
20. J. P. Ogilvie et al., "Use of coherent control for selective two-photon fluorescence microscopy in live organisms," *Opt. Express* **14**(2), 759–766 (2006).
21. B. Nie et al., "Generation of 42-fs and 10-nJ pulses from a fiber laser with self-similar evolution in the gain segment," *Opt. Express* **19**(13), 12074–12080 (2011).
22. V. V. Lozovoy et al., "Direct measurement of spectral phase for ultrashort laser pulses," *Opt. Express* **16**(2), 592–597 (2008).
23. B. Hou et al., "Compressor optimization with compressor-based multiphoton intrapulse interference phase scan (MIIPS)," *Opt. Lett.* **37**(8), 1385–1387 (2012).
24. G. Rasskazov et al., "Laser-induced phase shaping," *Phys. Rev. Appl.*, Submitted (2013).

Biographies of the authors are not available.